Magnetic field effects on coherent backscattering of light

R. Lenke[1,2,a] and G. Maret[1]

[1] University of Konstanz, Box 5560, 78457 Konstanz, Germany
[2] Institut Charles Sadron, 6 rue Boussingault, 67083 Strasbourg Cedex, France

Abstract. We have studied the influence of magneto-optical Faraday rotation on coherent backscattering of light experimentally, theoretically and by computer simulations of Monte-Carlo type. The consistency of these three approaches reveals new aspects of the propagation of vector waves in turbid media with and without Faraday rotation. Experimentally, we have demonstrated that the Faraday rotation may almost completely destroy the reciprocity of light paths. However, as shown by the simulations, the cone of coherent backscattering may not only be destroyed but also shifted off the exact backscattering direction, parallel to the magnetic field, as long as the amount of circular polarization is not completely destroyed by the multiple scattering. The relationship between coherent backscattering, depolarization and Faraday rotation are explained by a simple path model of vector waves. This leads to a new characteristic correlation length required to properly describe the influence of Faraday rotation on multiple light scattering.

PACS. 11.80.La Multiple scattering – 42.25.Dd Wave propagation in random media – 42.25.Hz Interference – 78.20.Ls Magnetooptical effects

1 Introduction

Coherent backscattering (CB) of waves in multiple scattering media has been well known for electrons [1] and light [2,3] for some time. During this period it has become more and more clear that CB is a fundamental effect in nature. CB is closely related to the fact that light paths are reversible, *i.e.* "if I can see you, you can see me". More precisely, it is closely related to the theorem of reciprocity [4], which states that the scattering matrix of the reversed path is the transposed matrix of the direct path. In the exact backscattering direction, a light path and its reversed path have exactly the same length and are thus always interfering constructively. This gives – theoretically – a backscattering enhancement of two [5]. In directions deviating slightly from the exact backscattering direction, this coherent backscattering enhancement disappears and the scattered intensity decreases to the 'normal' non-coherent intensity. The angular width of this so-called CB cone is proportional to the turbidity of the medium. The latter is quantified by the inverse length $1/\ell^\star$, $\ell^\star$ being the transport mean free path which is the characteristic step length of the random walk of the light in the medium. In the majority of cases, the cone width is generally smaller than about one degree. CB is present in any multiple scattering medium. It is a very 'stable' effect, *i.e.* it is not destroyed by the motion of the scatterers, nor by absorption, nor by a short coherence length of the incident light [6] (only the shape of the cone is liable to change but not its maximum

value); in fact, CB can even be observed with sunlight [7]. The only effect, which violates the theorem of reciprocity and thus destroys CB, is Faraday Rotation (FR) (and, closely related to it, magnetic dichroism). Of course, CB is destroyed by non-elastic scattering, *e.g.* by fluorescence or by relativistic moving scatterers. It is unclear so far to which extent CB influences (reduces) the diffusion constant of waves. This possible influence of CB on the diffuse light propagation is called 'weak localization'. In very strongly scattering media even a 'strong localization' of waves was predicted by Anderson [8].

The influence of FR on CB was initially predicted by Golubentsev [9] and MacKintosh and John [10]; these authors estimated that the effect should be very small. Nevertheless, we observed this effect for the first time experimentally [11–14] and fabricated samples in which FR almost completely destroys CB. Figure 1 displays an experimental example. However, our experimental results and the simulations of Martinez and Maynard [15,16] could not be fully explained by existing theories: we found, for example, that the influence of FR on CB should depend on the direction of the magnetic field and that the characteristic correlation length is only of the order of $\ell^\star$ [14].

Therefore, we developed a new path model which explains not only well the effects which had been observed so far but also new observations reported here. In the simulation part of this work we observed, for example, an angular shift of the CB cone off the exact backscattering which is accounted for by light incident perpendicular

a e-mail: ralf.lenke@uni-konstanz.de
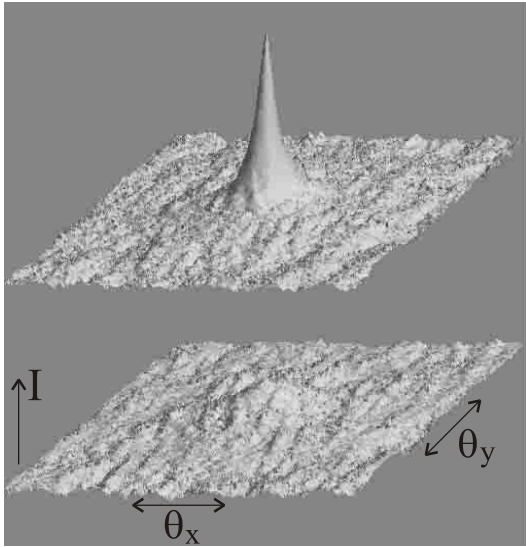
Fig. 1. CB cone at 0 tesla (above) and 23 teslas (below); intensity *versus* angle $\theta_{x,y}$ off exact backscattering direction. Angle section $0.15° \times 0.15°$. Without magnetic field the CB enhancement at $\theta_b = 0$ is 1.82, with magnetic field 1.30. Sample: molten, Faraday rotating glass powder mixed with 1% SiO$_2$ beads (radius $a = 90$ nm); $\ell^\star$ was estimated to $100\,\mu$m. Experimental conditions: room temperature, circular polarized light.

to the magnetic field direction. This model reveals that the influence of FR on CB is basically different in the regime of short light paths (of the order or shorter than the circular depolarization length) and the regime of relatively long light paths. Moreover, it gives an exact definition of a new characteristic length describing the influence of FR on multiple light scattering.

In this article we first briefly summarize the theory of CB, especially with respect to the relation between the reciprocity of light paths and the depolarization of light. A more detailed description of this part is found in [6]. Second, we present our model describing the influence of FR on CB. The validity of this model is then quantitatively verified by comparison with numerical simulations of Monte-Carlo type. Finally, we compare our (partially new) experimental data to the new theory and to simulations and find very good quantitative agreement.

2 Theory

2.1 Coherent backscattering

In multiple scattering samples, an incoming (light-) wave is scattered randomly numerous times. The outgoing wave can be explained as a superposition of many wavelets, corresponding to all possible light paths in the sample. Utilizing coherent light gives a typical interference pattern, the so-called speckle pattern [17] which alters quickly when the scatterers move. When averaging out various different configurations of the sample, these speckles disappear and the scattered intensity solely depends on 'geometrical' factors. This corresponds to the intensity which is obtained

after a non-coherent addition of all wavelets. However, in the exact backscattering direction one constructive interference effect survives this averaging, the so-called CB effect. CB is the interference between a multiple scattering light path and its reversed path (if existent in the setup) which, in itself, is not influenced by the movement of the scatterers, as both paths always have the same length. When considering scalar waves, this interference enhances the contribution to the intensity of each pair of paths, theoretically by a factor of two. Off the exact backscattering direction, a phase shift is introduced between the direct and the reversed path and the coherence – in the following denoted by $\mathcal{C}$ – between both paths decreases to zero with increasing angle of observation, *i.e.* increasing backscattering vector $\mathbf{q}_b := \mathbf{k}_{out} - (-\mathbf{k}_{in})$. Values of $\mathcal{C}$ can vary between -1 and 1; in the majority of cases, however, it is positive. At larger angles, the backscattered intensity corresponds to the 'incoherent' background ($\mathcal{C} = 0$). The shape of the normalized CB cone as a function of $\mathbf{q}_b$ is given by $1 + \frac{I_{ms}}{I_{ms}+I_{ss}} \mathcal{C}(\mathbf{q}_b)$. I_{ms} and I_{ss} are the (incoherent) intensities of the multiple scattering light paths and of single scattering, respectively. The pre-factor containing these intensities is necessary as single scattering does not contribute to CB and consequently reduces the enhancement factor of two. Its precise value depends on the incident and detected polarization state, the kind of scattering, absorption and on FR. The coherence $\mathcal{C}(\mathbf{q}_b)$ is the Fourier transform of the radial intensity distribution $I(\mathbf{r}')$ (with flux in the exact backscattering direction) at the surface of the sample around an illuminated spot at $\mathbf{r}' = 0$. The vector $\mathbf{r}'$ denotes the distance (in the surface) to the origin, *i.e.* the distance between beginning and end points of a light path [18] in the sample. Thus, one obtains [19,20]:

$$\mathcal{C}(\mathbf{q}_b) = \frac{1}{I_{ms}} \int_{r\neq 0}^{\infty} I(\mathbf{r}') \cos(\mathbf{q}_b \cdot \mathbf{r}') d\mathbf{r}' \qquad (1)$$

$$\approx \int_{s>0}^{\infty} p(s) \exp(-\frac{1}{3} s\,\ell^\star q_b^2) ds \;, \qquad (2)$$

$p(s)$ is the normalized probability distribution of all paths with length s. $I(\mathbf{r}')$ and $p(s)$ depend on the sample (type of scatterers, index of refraction etc.) and the polarization of light. The lower bounds of the integrals take into account the fact that single scattering does not contribute to CB [21]. Equation (2) is a diffusion approximation assuming that $\mathbf{r}'(s)$ has a Gaussian distribution around $\mathbf{r}' = 0$. The transport mean free path $\ell^\star$ is the characteristic length of the random walk and it is the distance over which the light loses, on average, the information about its initial direction. Approximately, this is also the average distance between beginning and end points of the light paths in backscattering geometry. Thus, the full width at half maximum of the cone should be of order $(\Delta q)_{FWHM} \approx 1/\ell^\star$ what can be verified by evaluating the integral in equation (2) [20]. With absorption, $p(s)$ must be replaced by the normalized probability distribution $p(s, \ell_a) \propto p(s) \exp(-s/\ell_a)$ where ℓ_a is the average

absorption length. In the diffusion approximation, equation (2), the curve shape with absorption is obtained from the curve shape without absorption by the replacement $q_b^2 \to q_b^2 + q_a^2$, $q_a^2 = 3/\ell_a\ell^\star$, and renormalization such that $\mathcal{C}$ is equal to 1 in the exact backscattering direction. This renormalization is necessary as absorption does not reduce $\mathcal{C}$.

Until now, we have only considered scalar waves. However, it is not evident that a correlation exists between the polarization on the direct and the reversed paths. In fact, for Rayleigh scattering it can be easily seen that the matrix $M_\odot$ (which describes the reversed path), is not the same as the matrix of the direct path $M_\otimes$ but that of the transposed matrix: $M_\otimes = M_\odot^T$. This correlation between the direct and reversed paths can be proved more generally, independent of the kind of scatterers, directly from *Maxwell's equations* and is known as the *theorem of reciprocity*. As a consequence, a factor of two can only be achieved if the incident and detected polarization states are equal (or if M is symmetric which, however, is not the case, in general). More generally, the incident polarization state $\mathbf{P}$ (detected polarization state $\mathbf{A}$, respectively) of the direct path must be equal to the detected (incident) polarization state of the reversed path. Only in this case the amplitude $e_\otimes$ on the direct path, given by $e_\otimes = \mathbf{A}M_\otimes\mathbf{P}$, is equal to the amplitude of the reversed path $e_\odot = \mathbf{P}M_\odot\mathbf{A} = \mathbf{P}M_\otimes^T\mathbf{A}$ for any light path represented by the matrix M. In the case of orthogonal detected polarization states there is no CB enhancement in the diffusion limit. However, due to the non-negligible amount of short paths (say less than ten scattering events) in backscattering direction, depending on the scatterers, the light may not be completely depolarized and there may be some CB enhancement also in the orthogonal polarization states. We will see that the depolarization plays an important role for the influence of FR on CB. We define the *remaining degree of linear and circular polarization* $\mathcal{P}_l$, $\mathcal{P}_c$ as following:

$$\mathcal{P}_l(s) = \frac{I_{\text{inc}}^{xx} - I_{\text{inc}}^{xy}}{I_{\text{inc}}^{xx} + I_{\text{inc}}^{xy}} \simeq \exp(-s/\ell_{p,l}) \qquad (3)$$

$$\mathcal{P}_c(s) = \frac{I_{\text{inc}}^{+} - I_{\text{inc}}^{\pm}}{I_{\text{inc}}^{+} + I_{\text{inc}}^{\pm}} \simeq \exp(-s/\ell_{p,c}), \qquad (4)$$

I_{inc} denoting the average incoherent multiple scattered intensities which are detected in the same linear (denoted by 'xx') or circular '$++$' polarization state and in the orthogonal ('xy' or '$\pm$') polarization states, respectively, than the incident light. Normally, a certain polarization state is destroyed exponentially with the characteristic average depolarization lengths $\ell_{p,l}$ and $\ell_{p,c}$. Depending on the scatterers, ℓ_p is of the order of $\ell^\star$ for Rayleigh or small Mie scatterers to some lengths of $\ell^\star$ for large Rayleigh-Gans-Debye scatterers. With these definitions one finds for the CB enhancement in the exact backscattering direction for the orthogonal channels [6] (in case of a rotational invariant sample with respect to $\mathcal{P}_l$):

$$\mathcal{C}_{q_b=0}^{\pm} = \left.\frac{2\mathcal{P}_l}{1 - \mathcal{P}_c}\right|_{\text{ms}} = \left.\frac{I_o\mathcal{P}_l}{I_{\text{inc}}^{\pm}}\right|_{\text{ms}} \qquad (5)$$

$$\mathcal{C}_{q_b=0}^{xy} = \left.\frac{\mathcal{P}_c + \mathcal{P}_l}{1 - \mathcal{P}_l}\right|_{\text{ms}} = \left.\frac{I_o\frac{1}{2}(\mathcal{P}_c + \mathcal{P}_l)}{I_{\text{inc}}^{xy}}\right|_{\text{ms}} \qquad (6)$$

$$\overline{\mathcal{C}}_{q_b=0} = \left.\frac{1 + \mathcal{P}_c}{2} + \mathcal{P}_l\right|_{\text{ms}}, \qquad (7)$$

'ms' indicates, that only the multiple scattering light paths (in backscattering direction) are taken into consideration, I_o is the total (unpolarized), incoherent backscattered intensity. Equation (7) represents the case of unpolarized light which is the weighted average value of the cases '$++$' and '$\pm$' (or 'xx' and 'xy'). The curve shapes of the CB cones in the different polarization states depend on $p(\mathbf{s})^{++}$, $p(\mathbf{s})^{\pm}$ etc. which may not only depend on the path length s but also on the configuration (denoted by $\mathbf{s}$) of a light path. In fact, the CB cone is not necessarily rotational invariant around the exact backscattering direction. The distributions $p(\mathbf{s})$, polarization included, can be obtained easily by Monte-Carlo simulations.

2.2 Coherent backscattering and Faraday rotation

FR rotates the polarization of light which propagates parallel to a magnetic field $\mathbf{B}$ by an angle $\Delta\alpha = V\mathbf{B} \cdot \boldsymbol{\Delta r}$ (clockwise with direction of observation against direction of propagation). The specific parameter V is the Verdet constant, $\boldsymbol{\Delta r}$ is the distance vector of propagation. In the case of circularly polarized light, this rotation corresponds to a positive or negative phase shift $\Delta\alpha_\sigma = \sigma\Delta\alpha = \sigma k_o(n_- - n_+)\Delta r$ for circular right ($\sigma = +1$, right-handed rotation in direction of propagation) or left ($\sigma = -1$) polarized light, respectively. Looking always in direction of propagation, $\Delta\alpha$ displays the opposite sign on the direct and the reversed paths. However, we are interested in following *Saxon's* notation, which does not change the coordinate system on the direct and the reversed path (only in this notation the matrix of the reversed path is just the transposed of the direct path). Then, $\Delta\alpha$ has the same sign on both paths. Thus the scattering matrices which describe the FR part in a multiple scattering light path are the same on the direct and the reversed paths but not the transposed matrices of each other as is required by the theorem of reciprocity. In fact, if FR is present, due to the external magnetic field $\mathbf{B}$, the multiple light scattering itself is no longer invariant to the transformation $\mathbf{r} \to -\mathbf{r}$ which is necessary for the reciprocity. With FR the total matrix describing the scattering path, is a mixture of matrices being the transposed, or the same on the reversed path, which generally obtains the result: $M_\odot(B) \neq M_\otimes^T(B)$. This inequality is necessary to destroy CB, however it is not sufficient as will be observed further on.

Until now, there is no exact analytical expression for the influence of FR on CB. Probably, this is due to the fact that FR acts on the amplitude (especially if the light amplitude is more linear polarized) as well as on the phase (in case of circular polarization) and both effects may not necessarily result in the same consequences for the CB cone. Moreover, on each segment of a light path,

the influence of FR on CB is correlated over a distance of about $\ell_{\mathrm{p,c}}$. This fact becomes even more important as in backscattering direction there are many short light paths. In the following we will try to explain the influence of FR on CB in a more illustrative way using different approaches. First we show up the difference between circular and linear polarized light, where we make the approximation that the light (even after scattering) always stays purely circular or linear polarized. Then we will present calculations where the polarization is treated correctly but where we still make the simplification that the scattering and FR are independent of each other. In a next step we will put emphasis on the correlation between FR and the scattering which leads to a new characteristic correlation length when FR is involved into multiple light scattering. In all these approaches we will neglect the fact that the light propagates in a half-infinite space. Nevertheless, these models explain well the simulated and measured results which will be presented in the following chapters.

So, let us make the approximation that the incident light is circularly polarized and does not change its polarization state by multiple scattering (this corresponds to a scalar wave approach). Between two scattering events, FR creates a phase shift of $\Delta\alpha_i = V\mathbf{B} \cdot \mathbf{\Delta r}_i$. For simplicity, we assume isotropic scattering, i.e. $\langle\Delta r\rangle = \ell^\star$. The total phase shift on a certain light path is $\alpha_{\mathrm{FR}} = \sum\Delta\alpha_i = V\mathbf{B} \cdot \sum\mathbf{\Delta r}_i = V\mathbf{B} \cdot \mathbf{r}$, where $\mathbf{r}$ is the distance vector between the starting and end points of the random walk. On the reversed path the phase shift has the opposite sign. Consequently, with FR, the phase shift $\mathbf{q}_{\mathrm{b}} \cdot \mathbf{r}'$ in equation (1) must be replaced by the phase shift $\mathbf{q}_{\mathrm{b}} \cdot \mathbf{r}' + 2\alpha_{\mathrm{FR}} = (\mathbf{q}_{\mathrm{b}} + 2\sigma V\mathbf{B}) \cdot \mathbf{r}'$, i.e. $\mathbf{q}_{\mathrm{b}} \to \mathbf{q}_{\mathrm{b}} + 2\sigma V\mathbf{B}$, where $\sigma = \pm 1$ is the handedness of the circular polarization. In the scalar wave approach the CB cone is not destroyed but shifted off the exact backscattering direction by a scattering vector $-2\sigma V\mathbf{B}$. In order to destroy CB, the light must be depolarized (this point will be discussed in more detail further below).

The circular polarization of the light is destroyed, on average, for path lengths $s > \ell_{\mathrm{p,c}}$. Approximately, this can be taken into consideration by assuming that, after the distance $\ell_{\mathrm{p,c}}$, the polarization of the light has flipped to the circular right or left polarization state with equal probability [10]. Thus, one obtains for the FR induced phase shift on a light path of n scattering events:

$$\begin{aligned}\alpha_{\mathrm{FR}} &= \sum_{\{n_p\}}\left(\pm\sum_{i=1}^{n_p}\Delta\alpha_i\right) &(8)\\ &= \sum_{\{n_p\}}\left(\pm\sum_{i=1}^{n_p}V\mathbf{B}\cdot\Delta\mathbf{r}_i\right) &(9)\\ &\xrightarrow[\text{average}]{\text{on}} \sum_{i=1}^{n}V\mathbf{B}\cdot\Delta\mathbf{r}_i^{\mathrm{FR}} = V\mathbf{B}\cdot\mathbf{r}_{\mathrm{FR}}\ . &(10)\end{aligned}$$

The inner sum represents the phase shift on path segments with length to the order of $\ell_{\mathrm{p,c}}$ (with n_{p} scattering events), the '$\pm$'-sign represents the random helicity flip of the circular depolarization after n_{p} scattering events.

These '$\pm$'-signs can be omitted on average over all path configurations; however, with the consequence that the total phase shift α_{FR} is no longer correlated with $\mathbf{q}_{\mathrm{b}} \cdot \mathbf{r}$ in equation (1) now. In order to denote this fact, the vectors $\mathbf{\Delta r}_i$ and $\mathbf{r}$ obtained the index 'FR'. Besides, we assume that there is no correlation between the helicity flip and the change of the direction of propagation. This is not always quite correct and will be discussed further below (anticipating the result of this discussion, we will see that, as a consequence of such correlations, the transport mean free path $\ell^\star$ must be replaced by a new characteristic length $\ell^\star_{\mathrm{FR}}$, which is only approximately equal to $\ell^\star$, in order to obtain the total FR induced phase shift).

Due to the helicity flips, $\mathbf{q}_{\mathrm{b}} \cdot \mathbf{r}$ and α_{FR} are no longer correlated and the cosine in equation (1) can be transformed, on average over all path configurations of length s as follows:

$$\langle\cos(\mathbf{q}_{\mathrm{b}} \cdot \mathbf{r} + 2\alpha_{\mathrm{FR}})\rangle = \langle\cos(\mathbf{q}_{\mathrm{b}} \cdot \mathbf{r})\rangle\langle\cos(2\alpha_{\mathrm{FR}})\rangle \quad (11)$$

$$\approx \exp\left[-\frac{1}{3}s\ell^\star q_{\mathrm{b}}^2\right]\exp\left[-\frac{1}{3}s\ell^\star_{\mathrm{FR}}(2VB)^2\right] \quad (12)$$

$$= \exp\left[-\frac{1}{3}s\ell^\star(q_{\mathrm{b}}^2 + q_{\mathrm{FR}}^2)\right] \quad (13)$$

$$\text{with}\qquad q_{\mathrm{FR}}^2 = \frac{\ell^\star_{\mathrm{FR}}}{\ell^\star}(2VB)^2\ . \quad (14)$$

In the first line we used the independence of $\mathbf{r}$ and α_{FR} and $\langle\alpha_{\mathrm{FR}}\rangle = 0$. The factor 2 in front of α_{FR} derives from the (same) phase shift on the direct and the reversed path. The second exponential term in line (12) is obtained in analogy to the first one (transformation of Eqs. (1)→(2)) by assuming that the FR induced phase shift makes a random walk with step length $VB\mathbf{\Delta r}_{\mathrm{FR}}$ where $\langle\Delta r_{\mathrm{FR}}\rangle = \ell^\star_{\mathrm{FR}}$. This result which was essentially obtained by and used in former works [9–13] is in more or less qualitative agreement with experimental results. Assuming an exponential distribution of Δr_{FR}, this result can also be obtained by the transformation

$$\langle\cos(2\sum\Delta\alpha_i)\rangle = \langle\cos(2\Delta\alpha)\rangle^n \overset{(\mathrm{a})}{=} \quad (15)$$
$$\left[\frac{\arctan(2VB\ell^\star_{\mathrm{FR}})}{2VB\ell^\star_{\mathrm{FR}}}\right]^n \overset{(\mathrm{b})}{\approx} \exp[-\frac{1}{3}s\ell^\star_{\mathrm{FR}}(2VB)^2]\ ,$$

where we made use of the independence of the phase shifts $\Delta\alpha_i$ and their symmetry around zero. The approximation (15b) is the better the smaller $\Delta\alpha$ and/or the larger n. For short paths and/or larger $\Delta\alpha$, a better approximation is given by evaluating equation (15a), resulting in $q_{\mathrm{FR}}^2 = 3/(\ell^\star\ell^\star_{\mathrm{FR}})\ln[\arctan(2VB\ell^\star_{\mathrm{FR}})/(2VB\ell^\star_{\mathrm{FR}})]$ which was used in [14]. Obviously, for some samples, this approximation already fits quite well.

Consequently, the shape of the CB cone with FR is obtained by the replacement $q_{\mathrm{b}}^2 \to q_{\mathrm{b}}^2 + q_{\mathrm{FR}}^2$. Quite similar to absorption, FR cuts off the longer paths and rounds off the top of the cone. However, in contrary to absorption, the incoherent background is not changed and the CB cone is destroyed.

Until now we used a (helicity flip) model where we assumed that the polarization of the light can only occupy

the circular eigen-states. However, when using linearly polarized incident light and a sample of Rayleigh scatterers, the light will stay linearly polarized all along the light path. In this case, instead of a phase shift, a rotation of the polarization of the light is introduced by FR. Finally, this will result in different absolute values of the amplitudes $e_\otimes$ and $e_\odot$. This mechanism of the influence of FR on CB is closely related to the fact that, with the assistance of FR, it is possible to build an optical diode which permits the possibility: "I can see you, but you cannot see me". An optical diode is composed of two linear polarizers twisted by $45°$ with a material with a FR of $45°$ in between. The light is able to pass this isolator in one direction, but not in the other. Rayleigh scatterers for example, polarize the light, especially if the light is scattered under $90°$. Therefore, it is possible to imagine an optical diode built up of Rayleigh scatterers which are embedded in a FR material (in contrary to an optical isolator, the light is not absorbed but is scattered in a different direction). Of course, scatterers in a turbid sample do not correspond to a perfect optical diode, but to an imperfect diode. As a consequence, the amplitudes on a pair of paths are influenced differently and CB decreases. In some sense, by imaging that the light paths in a turbid sample resemble a heap of spaghetti, with FR, the heap of the direct paths will become different from the heap of the reversed paths.

So far, we explained with 'hand-waving' arguments the influence of FR on CB for the extreme cases of purely circular and purely linear polarized light. Of course, reality lies in-between. Combining the influence of FR on phase and amplitude one obtains instead of equation (2):

$$\mathcal{C}(\mathbf{q_b}, V\mathbf{B}) = \tag{16}$$

$$\frac{1}{I_{ms}} \int I_b(\mathbf{r}) \frac{2|e_\otimes||e_\odot|}{|e_\otimes|^2 + |e_\odot|^2} \cos(\mathbf{q_b} \cdot \mathbf{r} + 2\alpha_{FR}) d\mathbf{r}$$

$$\approx \frac{1}{I_{ms}} \int I_b(\mathbf{r}) \underbrace{\frac{2\Re[e_\otimes e_\odot^*]}{|e_\otimes|^2 + |e_\odot|^2}}_{\stackrel{(b)}{=:} \mathcal{C}(V\mathbf{B},\mathbf{s})} \cos(\mathbf{q_b} \cdot \mathbf{r}) d\mathbf{r} \tag{17}$$

where '$*$' denotes the complex conjugate, $\Re$ the real part. The term $\mathcal{C}(V\mathbf{B},\mathbf{s})$ reflects the coherence in the exact backscattering direction between the direct and the reversed path $\mathbf{s}$ as a function of FR. It does not only depend on $\mathbf{r}$ but also on the configuration of the path. The approximation (17) is obtained after the replacement [24] $\cos(\mathbf{q_b} \cdot \mathbf{r} + 2\alpha_{FR}) = \cos(\mathbf{q_b} \cdot \mathbf{r}) \cos(2\alpha_{FR}) - \sin(\mathbf{q_b} \cdot \mathbf{r}) \sin(2\alpha_{FR})$ and is only valid if the second term is on average zero, *i.e.* if there is no correlation between $\mathbf{q_b} \cdot \mathbf{r}$ and α_{FR}. Generally, this is only true if $\mathbf{B} \parallel \mathbf{k_{in}}$.

In the following we present the analytical calculations of $\mathcal{C}(VB, s)$ for the different polarization states, where we made the following approximations: (i) The light paths are divided into pieces of average length $\ell_{FR}^\star$ which were represented by the 2×2 scattering matrices S_i. These matrices are supposed to be identical on average over all path configurations. (ii) Between those scattering events the wave experienced a FR of $\Delta\alpha_i$ (represented by rotational matrices F_i). (iii) All matrices are independent of

each other. (iv) Only light paths in an infinite medium without boundaries are considered. (v) The matrices S_i are independent of the magnetic field which will be discussed in the Appendix in more detail.

Still, the matrices S_i fulfill the theorem of reciprocity and they have, on average over all path configurations (indicated by $\langle . \rangle$), the following symmetries [6]:

$$\langle|\mathsf{S}_{11}|^2\rangle = \langle|\mathsf{S}_{22}|^2\rangle, \quad \langle|\mathsf{S}_{12}|^2\rangle = \langle|\mathsf{S}_{21}|^2\rangle, \tag{18}$$

$$\langle\Re[\mathsf{S}_{11}\mathsf{S}_{22}^* + \mathsf{S}_{12}\mathsf{S}_{21}^*]\rangle = -\langle|\mathsf{S}_{11}|^2 - |\mathsf{S}_{12}|^2\rangle, \tag{19}$$

$$\langle\mathsf{S}_{11}\mathsf{S}_{12}^*\rangle = -\langle\mathsf{S}_{21}\mathsf{S}_{22}^*\rangle, \quad \langle\mathsf{S}_{11}\mathsf{S}_{21}^*\rangle = -\langle\mathsf{S}_{12}\mathsf{S}_{22}^*\rangle, \tag{20}$$

which follow from the assumption that the scatterers are distributed isotropically and that the results should be indifferent to a rotation of the system. The following relations (21–24) between $\mathcal{C}$ and $\mathcal{P}$ have been obtained by setting $\mathsf{M} = \mathsf{S}_n\mathsf{F}_n...\mathsf{S}_2\mathsf{F}_2\mathsf{S}_1\mathsf{F}_1$ and by evaluating equations (3, 4) and (17b). They have been proved by recursion in the number of scatterers and Faraday rotations. We obtain for both $n = s/\ell_{FR}^\star$ independent scatterers and n independent Faraday rotations $\Delta\alpha_i$, in the case of circularly polarized incident and detected light $(++)$ on average over all path configurations:

$$\mathcal{C}(VB, s)^{++} = \langle\cos(2\Delta\alpha_i)\rangle^n \tag{21}$$

which is the exact same result as obtained by the helicity flip model, equations (11–15).

For the linear polarization we obtain with the same approximations

$$\mathcal{C}(VB, s)^{xx} = \frac{\mathcal{P}_1(s) + \mathcal{C}(VB, s)^{++}}{1 + \mathcal{P}_1(s)\mathcal{C}(VB, s)^{++}}. \tag{22}$$

The term $\mathcal{P}_1(s)$ was defined in equation (3). It is the depolarization in absence of a magnetic field, *i.e.* without FR. With magnetic field, the linear depolarization $\mathcal{P}_1(s, VB)$ is given by $\mathcal{P}_1(s)\mathcal{C}(VB, s)^{++}$ as can be seen directly from the denominator in equation (22).

Consequently, contrary to $\mathcal{C}(VB, s)^{++}$ which ranges from 1 to 0, in the case of linear polarization, the extent to which CB is destroyed by FR, depends on the depolarization of the linear polarization state. If the light is not depolarized, as may it be the case in two dimensional samples (polarization perpendicular to the scattering plane), $\mathcal{C}^{xx}$ is not influenced at all by FR. This result can also be explained with the model described above, *e.g.* by decomposing the linear polarization state in a circular left and right polarized wave: if the linear polarization state is not destroyed, both circular states will be completely correlated and experience the same phase shift but of opposite sign all over the path; consequently FR has no effect. In equation (22), the denominator and thus the path length distribution $p(s)$, which is necessary to calculate the shape of the cone, is magnetic field dependent. Additionally, the amount of single scattering may change. Strictly speaking, and only in the case '$++$', the shape of the cone with FR can consequently be explained by the substitution $q_b^2 \to q_b^2 + q_{FR}^2$. However generally, and especially for long paths, the term $\mathcal{P}_1(s)$ is rather insignificant

and negligible. Within this approximation we achieve the same expressions for $\mathcal{C}^{xx}$ and $\mathcal{C}^+$.

For crossed circular polarizer and analyzer we obtain

$$\mathcal{C}(VB, s)^\pm = \frac{2\mathcal{P}_l(s)}{1 - \mathcal{P}_c(s)} . \tag{23}$$

Thus, $\mathcal{P}_c(s)$ which was defined in equation (4), and the opposite circular polarized cone, if existent, are not influenced by FR. The latter corresponds to an analytical prediction of MacKintosh and John [10] and to numerical simulations of Martinez and Maynard [15,16]. It can be understood in the helicity flip model as follows: if a helicity flip occurs during a scattering event on the direct path, due to reciprocity, a helicity flip must also occur on the reversed path. As the incident and detected polarization states are orthogonal ($\mathcal{C}^\pm$), the polarization of the direct path is always orthogonal to the polarization of the reversed path (in the helicity flip model only the states '+' and '−' are allowed). As also the orientation with respect to the magnetic field is reversed on the reversed path, it follows that $\alpha_{\mathrm{FR}}^\odot = \alpha_{\mathrm{FR}}^\otimes$.

For opposite linear polarized states (xy) we achieve:

$$\mathcal{C}(VB, s)^{xy} = \frac{\mathcal{P}_l(s) + \mathcal{P}_c(s)\mathcal{C}(VB, s)^+}{1 - \mathcal{P}_l(s)\mathcal{C}(VB, s)^+} . \tag{24}$$

As a consequence, if there is a cone in the opposite linear polarized state, it is influenced by FR. However, if the external magnetic field is parallel to the incident light, this effect is superimposed on a boundary effect: the first step of the light penetrating into the sample can be considered as a ballistic propagation. On this step FR acts on all paths in the same way, which can be considered as a collective rotation of the polarization of the cone. This rotation can be compensated for by a corresponding rotation of the analyzer. We will discuss this effect more precisely in the section including the Monte-Carlo simulations.

Expressions (22–24) can be integrated over all path lengths s:

$$\mathcal{C}(VB)^\pm = \left. \frac{2\mathcal{P}_l}{1 - \mathcal{P}_c} \right|_{\mathrm{ms}} \tag{25}$$

$$\mathcal{C}(VB)^{xx} = \left. \frac{\mathcal{P}_l + \mathcal{C}(VB)^+}{1 + \mathcal{P}_l\mathcal{C}(VB)^+} \right|_{\mathrm{ms}} \tag{26}$$

$$\mathcal{C}(VB)^{xy} = \left. \frac{\mathcal{P}_l + \mathcal{P}_c\mathcal{C}(VB)^+}{1 - \mathcal{P}_l\mathcal{C}(VB)^+} \right|_{\mathrm{ms}} \tag{27}$$

$$\overline{\mathcal{C}}(VB) = \mathcal{P}_l + \left. \frac{1 + \mathcal{P}_c}{2}\mathcal{C}(VB)^+ \right|_{\mathrm{ms}} . \tag{28}$$

In the case of $VB \to \infty$, i.e. $\mathcal{C}(VB)^+ = 0$, the expressions $\mathcal{C}^{xx}$, $\mathcal{C}^{xy}$ and $\overline{\mathcal{C}}$ have the consistent value $\mathcal{P}_l$ and in the case $VB \to 0$ we obtain equations (5–7).

To summarize, within the approximation that the scattering and FR are independent of each other, we found a simple relationship between CB, FR and the depolarization of light. As will be seen from the Monte-Carlo simulations of 'real' cases, these relationships are not fulfilled

exactly. However, qualitatively, they explain the results rather well. Without magnetic field, the relations between CB and $\mathcal{P}$ are always exact [6].

In analogy to this analytical evaluation of the influence of FR on CB, we have also studied the influence of optical activity in multiple scattering samples. Naturally, $\mathcal{C}^{xx}$ and $\mathcal{C}^+$ are not influenced, since optical activity follows the theorem of reciprocity. $\mathcal{C}^{xy}$ and $\mathcal{C}^\pm$ are influenced to the extent that $\mathcal{P}_l$ decreases with increasing optical activity. $\mathcal{P}_c$ remains unchanged under optical activity.

Now we want to discuss a possible correlation between (i) the influence of FR on CB, (ii) the random walk of the waves and (iii) the depolarization of light. Let us consider one Rayleigh scattering event, circular polarization and $\mathbf{k}_{\mathrm{in}} \parallel \mathbf{B}$. In this case, if the light is scattered in backward direction, FR changes sign as the direction of propagation changes with respect to $\mathbf{B}$. This change of sign is compensated for by the fact that the polarization flips to the opposite circular polarization state. Thus, FR is added up after reflection and is not compensated for, as is the case for optical activity. In what concerns the randomization of the FR induced phase shift $\Delta\alpha_{\mathrm{FR}}$, there is no difference if the wave is reflected or if it goes straight ahead (especially in this case, FR is not randomized by such a scattering event). This idea, which is the basic point of this model, can be generalized independently of the orientation of $\mathbf{B}$: from the point of view of FR, a scattering angle θ, if combined with a helicity flip, is equivalent to a scattering angle $\theta - \pi$ without helicity flip. So, if the wave experiences a change of the circular polarization state, we will replace the scattering angle θ by $\theta - \pi$ and keep the original polarization state. Thus we get rid of the correlation between the random walk and FR. In the following, this procedure will also be applied if the wave is not in a pure circular polarization state after scattering. Thereto, the scattered amplitude is decomposed into the two circular polarized eigen-states and the above described operation is applied to the part of the intensity which was scattered into the opposite state. In the representation of circular eigen-states (denoted by '$\pm$') the scattering matrix of Rayleigh scattering $\mathsf{S}(\theta) = \begin{pmatrix} 1 & 0 \\ 0 & \cos\theta \end{pmatrix}$ takes the form $\mathsf{S}(\theta)_\pm = \frac{1}{2} \begin{pmatrix} \cos^2(\theta/2) & \sin^2(\theta/2) \\ \sin^2(\theta/2) & \cos^2(\theta/2) \end{pmatrix}_\pm$. Consequently, an incoming circular polarized wave, e.g. $(1, 0)_\pm$, is depolarized by the scattering to $\frac{1}{2}(\cos^2(\theta/2), \sin^2(\theta/2))_\pm$. So, the wave is scattered in the direction of θ, with polarization $(1, 0)_\pm$, with a probability proportional to $[\cos^2(\theta/2)/2]^2$ and with the polarization $(0, 1)_\pm$ with a probability $\propto [\sin^2(\theta/2)/2]^2$. Following the operation described above, the scattering angle θ is replaced by $\theta - \pi$ for the part $(0, 1)_\pm$ which, afterwards, is attributed to the part $(1, 0)_\pm$ again. This procedure corresponds to a modified helicity flip model as only pure eigen-states of the circular polarization are considered. With respect to the correlations of FR on a multiple scattering light path, the scattering amplitude in 'FR-space' is given by $(\cos^2[\theta/2] + \sin^2[(\theta - \pi)/2])/2 = \cos^2(\theta/2)$; the first and second term representing the probability that the light either stays in the same

polarization state, or respectively experiences a helicity flip. With 'FR-space' we want to emphasize that, after the substitution $\theta \to \theta - \pi$, the position of the wavelet, corresponding to the influence of FR, does no longer correspond to the position in the sample. The coordinates in FR-space will be indicated by 'FR'. The 'differential cross-section' from the point of view of FR, is $\cos^4(\theta/2)$, whereas the differential cross-section in 'real' space is $(1 + \cos^2 \theta)/2$. In analogy to the definition of the length $\ell^\star$ in case of anisotropic scattering, one can define a correlation length $\ell^\star_{\mathrm{FR}} = \ell/(1 - \langle \cos \theta_{\mathrm{FR}} \rangle)$ for the influence of FR on CB where the differential cross-section in FR-space is used. For Rayleigh scattering one obtains $\ell^\star_{\mathrm{FR}} = 2\ell$, *i.e.* the influence of FR on CB is two times stronger than expected from former theories.

In the model described above, due to the circular depolarization of the light, a multiple scattering light path is split up into a whole bunch of independent light paths. This procedure is correct as long as there is no correlation between the two circular eigen-states. In order to verify the range of validity of this model we compared (by numerical simulations) the destruction of $\mathcal{C}(VB, s)^{+}$ in real space with the propagation in FR-space (with the corresponding modified cross-section) as a function of VB and the number of scattering events n. According to our model, in FR-space, the influence of FR on CB just corresponds to a simple phase shift given by $\alpha_{\mathrm{FR}} = VB \cdot \mathbf{r}_{\mathrm{FR}}$, whereas the influence of FR on CB in real space, especially due to possible correlations between $\Delta\alpha$ and $\mathbf{S}$, is more complicated. We made the approximation of an infinite medium with no boundaries, corresponding to paths which start and end somewhere within the sample. This approximation is justified by the fact that we essentially want to study the validity of the modified cross-section model, *i.e.* justify the necessity of the new length $\ell^\star_{\mathrm{FR}}$ which is a parameter being defined in the diffusion limit. All other effects, *e.g.* the differences in $\mathcal{C}^{+}$ and $\mathcal{C}^{xx}$, vanish in the diffusion limit but not the difference between $\ell^\star_{\mathrm{FR}}$ and $\ell^\star$. The procedure was the following: in FR-space we always 'followed' the same (incident) circular polarization state, which might experience helicity flips (due to depolarization). After the last scattering event, we counted only those light paths which would have arrived with the same circular polarization state as incident (*i.e.* experienced an even number of helicity flips). As already mentioned above, in FR-space, a phase shift of $\alpha_{\mathrm{FR}} = VB \cdot \mathbf{r}_{\mathrm{FR}}$ is introduced by FR, where $\mathbf{r}_{\mathrm{FR}}$ is the propagated distance between beginning and end point of a light path in FR-space. As in FR-space only the phase but not the absolute value of the amplitude is changed ($|e_\odot| = |e_\otimes|$) the coherence $\mathcal{C}(VB, s)^{+}_{\mathrm{FR}}$ of circular polarized waves, between the direct and the reversed paths, decreases as a function of FR like

$$\mathcal{C}(VB, s)^{+} = \int W(\mathbf{r}_{\mathrm{FR}}) \cos(2VB \cdot \mathbf{r}_{\mathrm{FR}}) \mathrm{d}\mathbf{r}(\mathbf{s}), \qquad (29)$$

where $W(\mathbf{r}_{\mathrm{FR}})$ is the intensity distribution around the starting point of the random walk, for scatterers which are modified according to the correlation between FR and the scattering. Equation (29) is also the definition of the
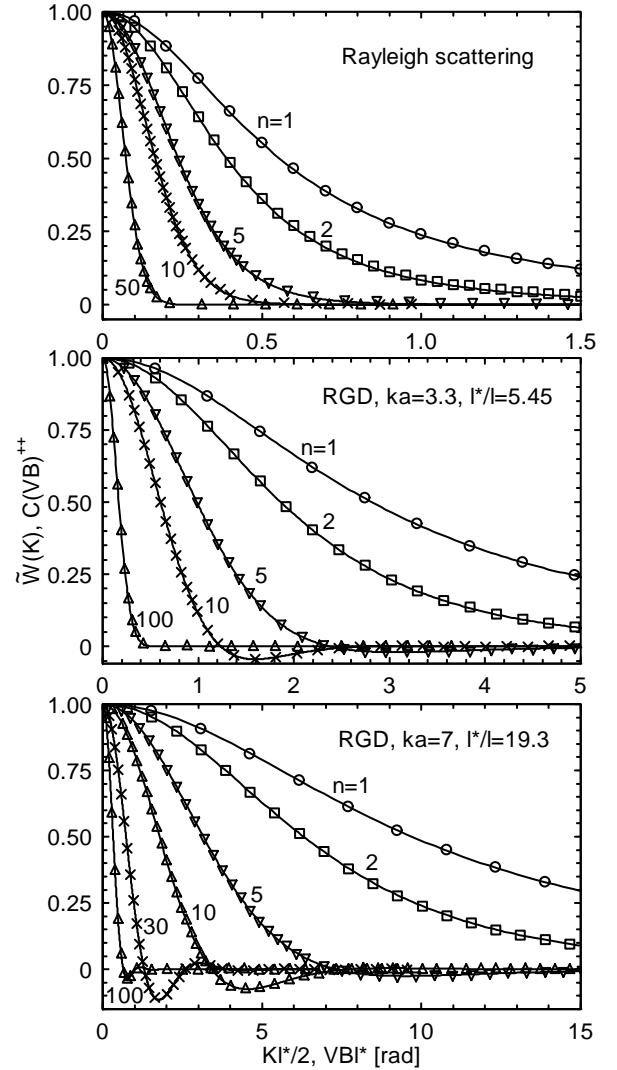
Fig. 2. Upper plot: Rayleigh scattering. Lower plots: Rayleigh-Gans-Debye scattering with size parameters $ka = 3.3$ and $ka = 7$. Points: simulated decrease of coherence $\mathcal{C}^{+}$ between a multiple scattering light path and its reversed path in a sample without boundaries, for different numbers n of scatterers and $n + 1$ steps in a Faraday rotating media, as a function of VB. Lines: Fourier transform $\widetilde{W}(K)$ of the end-to-end point distribution of the same paths in 'FR-space'. These figures clearly demonstrate that the interpretation of the influence of FR on CB by the modified scattering matrices fits very well.

characteristic function $\widetilde{W}(\mathbf{K}, s) := \int W(\mathbf{r}) \cos(\mathbf{K} \cdot \mathbf{r}) \mathrm{d}\mathbf{r}$ of the random walk, if $2VB$ is replaced by $\mathbf{K}$. So, in order to verify our model, we simulated a random walk with the modified scatterers and calculated numerically the characteristic function $\widetilde{W}(\mathbf{K})$. Finally, we compared this curve with the curve $\mathcal{C}(VB, s)^{+}$, according to its definition in equation (17), which was obtained by Monte-Carlo simulations for the scatterers in real space. Figure 2 shows the results for different numbers of scatterers, *i.e.* for different path lengths. In any case, the coincidence is amazingly good. There is a minor difference of about 5% for less than 10 scatterers and relatively large values of $VB\ell^\star$ which will be discussed further below.
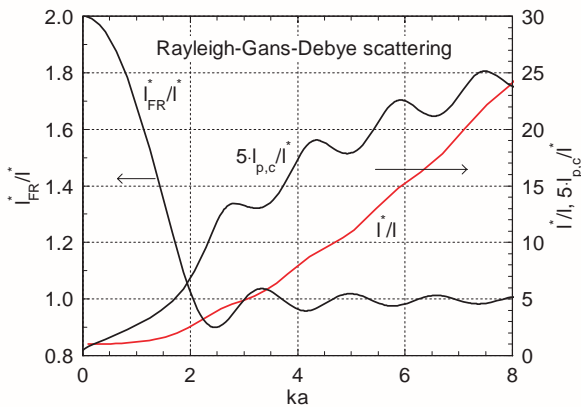
Fig. 3. Numerical calculation of $\ell_{\mathrm{FR}}^{\star}/\ell^{\star}$ as a function of the size parameter ka. The characteristic length $\ell_{\mathrm{FR}}^{\star}$ is calculated in analogy to the definition of $\ell^{\star}$; it is different from $\ell^{\star}$ as the anisotropy in 'FR-space' is different from the anisotropy in real space. Also the circular depolarization length $\ell_{\mathrm{p,c}}$ is calculated numerically (curve is stretched by a factor of 5).

We also studied Rayleigh-Gans-Debye scattering. In this case, for the differential cross section in FR-space one obtains: $\cos^4[\theta/2](F[\theta]+F[\theta-\pi])/2$ where $F[\theta]$ is the form factor [25]. Figure 2 shows the results from the simulations for different size parameters. Again, the coincidence is very good. In fact, the small difference in the case of Rayleigh scattering diminishes with increasing size parameter. In figure 3 the correlation length $\ell_{\mathrm{FR}}^{\star}$ is plotted for Rayleigh-Gans-Debye scattering as a function of the size parameter ka (wave vector times particle radius).

This analogy between the influence of FR on CB and a random walk in FR-space is not generally true for a single light path, rather only on average over all possible configurations of the light paths of a certain length. This is due to the fact that FR also changes the amplitude, *i.e.* the probability of a certain light path, what was not explicitly taken into account in this model. In other words, the correlation between the two circular polarization states (*i.e.* between the bunches of light paths mentioned above), which we did not take into consideration in this model, is only negligible on average in all configurations of the light paths. However, after this averaging, this model matches quite well, even for short paths. The smaller the size parameter of the scatterers, the stronger the influence of the scattering on the polarization, *i.e.* the amplitude of the light. Rayleigh scatterers even linear polarize the light by scattering under 90° and thus create, to some extent, a correlation between the two circular polarization states. Obviously, this is the reason for the small discrepancy in our model in regards to Rayleigh scattering.

With this model one can also understand possible correlations between $\mathbf{q}_{\mathrm{b}} \cdot \mathbf{r}$ and α_{FR}. As explained in the beginning, in the extreme case where the incident circular polarization is not destroyed, $\mathbf{q}_{\mathrm{b}} \cdot \mathbf{r}$ and α_{FR} are completely correlated, resulting in a shift of the top of the cone away from the exact backscattering direction. But in this case, the trajectory in FR-space and real space are identically. Obviously, this statement can be

generalized: $\mathbf{q}_{\mathrm{b}} \cdot \mathbf{r}$ and α_{FR} are the less correlated the more different are the trajectories in FR-space and real space. By definition, these trajectories become different after the distance $\ell_{\mathrm{p,c}}$ (characteristic circular depolarization length), *i.e.* the correlation is completely destroyed after several lengths of $\ell_{\mathrm{p,c}}$. Generally, for spherical particles, the larger the size parameter ka, the longer the circular depolarization length $\ell_{\mathrm{p,c}}$ with respect to $\ell^{\star}$ (see Fig. 3) and consequently, the stronger the correlation. This has dramatic consequences for the influence of FR on the CB cone as is exemplified in the Monte Carlo simulations.

To summarize, due to the symmetry breaking of the external magnetic field, FR influences phase and amplitude of the light on the direct and reversed paths differently. In the diffusion limit, this influence can be reduced to random changes of the complex light amplitude on pieces of paths with the average correlation length $\ell_{\mathrm{FR}}^{\star}$. On each segment, these changes correspond to a difference in phase of $2\Delta\alpha$ between the direct and reversed path, with $\langle(2\Delta\alpha)^2\rangle = \frac{2}{3}(2VB\ell_{\mathrm{FR}}^{\star})^2$. For Rayleigh-Gans-Debye scattering, one finds for the FR correlation length $0.9 \lesssim \ell_{\mathrm{FR}}^{\star}/\ell^{\star} \leq 2$. Below the diffusion limit one can differentiate between the cases where the path lengths are shorter or longer than about $\ell_{\mathrm{p,c}}$. For shorter paths, there is a correlation between the angular dependence of the CB cone, *i.e.* $\mathbf{q}_{\mathrm{b}} \cdot \mathbf{r}$ and the FR induced phase shift α_{FR} resulting in the substitution $\mathbf{q}_{\mathrm{b}} \to \mathbf{q}_{\mathrm{b}} + 2\sigma V\mathbf{B}$. For long paths (diffusion limit), the substitution is $q_{\mathrm{b}}^2 \to q_{\mathrm{b}}^2 + (\ell_{\mathrm{FR}}^{\star}/\ell^{\star})(2VB)^2$. For the short paths, one finds also a difference between $\mathcal{C}^{+}$, $\mathcal{C}^{xx}$, $\mathcal{C}^{\pm}$ and $\mathcal{C}^{xy}$ as long as the light is not yet completely depolarized. This model gives a qualitative picture of the influence of FR on CB. The reality, due to the backscattering geometry, is a mixture of short and long paths (about 50% of the light is scattered less than 10 times) and, additionally, the light paths must fulfill the boundary condition of starting and ending at the surface of the sample. Therefore, complete analytic expressions for the influence of FR on the shape of the CB cone are very difficult.

3 Monte-Carlo simulations

In order to better understand the influence of FR on CB and in order to verify the predictions that we have obtained in the theoretical part, we made numerical simulations of Monte-Carlo type. The first simulations on this topic were carried out by Martinez and Maynard [15,16]. They studied the cases of Rayleigh and Mie scatterers which were embedded in a FR material. However, contrary to their work, we not only studied the intensity in the exact backscattering direction but the entire shape of the cone, which proved to be interesting due to the correlations mentioned in the previous section. Moreover, we also introduced into our simulations real experimental parameters such as limited sample thickness, limited resolution of the setup and importantly, the mismatch of the index of refraction at the surface, which was absolutely necessary to obtain a firm agreement with our
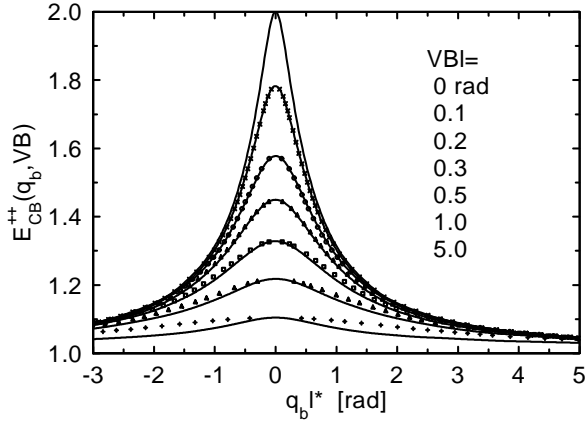
Fig. 4. Monte-Carlo simulation of CB enhancement E_{CB} as a function of $q_b\ell^\star$ for Rayleigh scattering, circular polarization, $\mathbf{B} \parallel \mathbf{k}_{in}$ and an absorption length of $\ell_a = 100\ell^\star$. Solid lines: Simulations for different $VB\ell^\star$. Dots: curve at zero field rescaled by $q_b^2 \rightarrow q_b^2 + q_{FR}^2$, where q_{FR} is given according to the maximum value of each curve. Up to values of $VB\ell^\star \approx 0.5$ rad the rescaled curves match quite well.

experimental results. In the case of anisotropic scattering, we restricted ourselves to Rayleigh-Gans-Debye scattering because basic differences, when compared to isotropic scattering, are due to the fact that $\ell^\star$ is longer than the scattering mean free path ℓ and that the characeristic depolarization lengths, especially $\ell_{p,c}$, are relatively long compared to $\ell^\star$. The first condition is fulfilled for both Rayleigh-Gans-Debye and Mie scattering, the second condition is a little bit more pronounced for Rayleigh-Gans-Debye scattering. Nevertheless, there should be no basic differences between Rayleigh-Gans-Debye and Mie scattering.

We used the technique of 'partial photons' [6,26] which is very well suited to the problem of CB as the angular width of the CB cone is smaller than 1°, normally. On each occasion, we averaged more than $\approx 10^5$ light paths, sufficient to reduce the fluctuations below 1%. As in the theoretical section, we assumed that FR acts only on the coherent wave between two scattering events, *i.e.* we neglected the influence of FR on the scattering itself (see Appendix).

3.1 Rayleigh scattering

Figure 4 shows a simulation of circular polarized light, in the case where the magnetic field $\mathbf{B}$ is parallel to the incident light. It corresponds more or less to the predictions of former authors, *i.e.* CB decreases with increasing FR and the shape of the cone can be described essentially by the substitution $q_b^2 \rightarrow q_b^2 + q_{FR}^2$. However, the functional dependence of q_{FR} on VB is not trivial. In fact, the diffusion approximation, where $q_{FR}^2 = (\ell_{FR}^\star/\ell^\star)(2VB)^2$ with $\ell_{FR}^\star/\ell^\star = 2$, see equations (13, 14), is only valid for very small values of $VB\ell^\star$, *i.e.* $q_{FR} \lesssim 0.1$. This is due to the fact that in backscattering geometry there are many short paths in which the diffusion approximation is very bad.
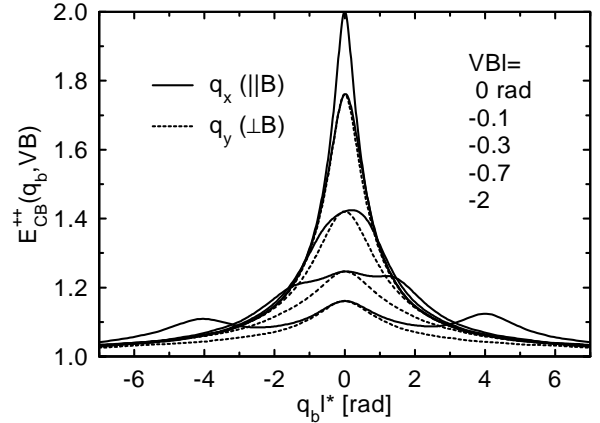
Fig. 5. Same situation as in Figure 4, but $\mathbf{B} \perp \mathbf{k}_{in}$. In direction of the magnetic field (solid lines) secondary maxima appear and the curves become slightly asymmetric. Dashed lines: $\mathbf{q}_b \perp \mathbf{B}$.
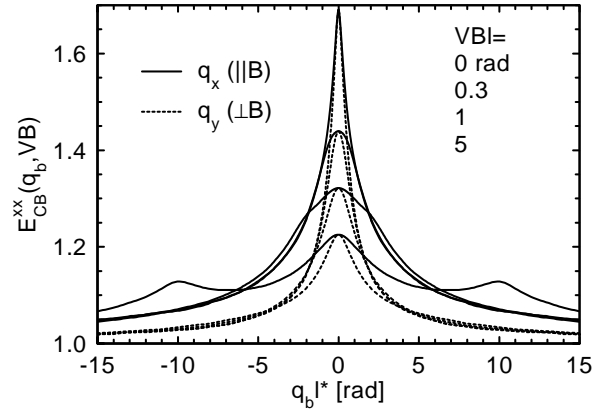
Fig. 6. Same situation as in Figure 5, but linear polarization. Again, in direction of the magnetic field (solid lines) secondary maxima appear but the curves stay symmetric.

Figures 5 and 6 show the results for the CB enhancement, $E_{CB} := 1 + \frac{I_{ms}}{I_{ms+ss}}\mathcal{C}$, for the cases '++' and 'xx' with the magnetic field perpendicular to the incident light. In both cases, two secondary maxima appear with increasing FR. Moreover, E_{CB}^{++} becomes slightly asymmetrical. We will expand upon this topic further on, in context with Rayleigh-Gans-Debye scattering.

The case of linear polarization and $\mathbf{B} \parallel \mathbf{k}_{in}$ is quite special. If measured in the usual way, E_{CB}^{xx} will decrease rather quickly, but E_{CB}^{xy} will increase with increasing FR. This behavior is explained by the light penetrating a distance of about one $\ell^\star$ more or less ballistically into the sample. At this distance, FR can be understood to be like the rotation in a window of the sample holder which can be compensated for by a rotation of the analyzer by an angle to the order of $\beta' = 2VB\ell^\star$. In a more precise (but still simplified) model we assume that (i) the first and last step into and out of the sample, *i.e.* the distances of the starting and end points of the random walk from the surface, are independent of each other; (ii) that these distances are distributed exponentially and (iii) that the light paths
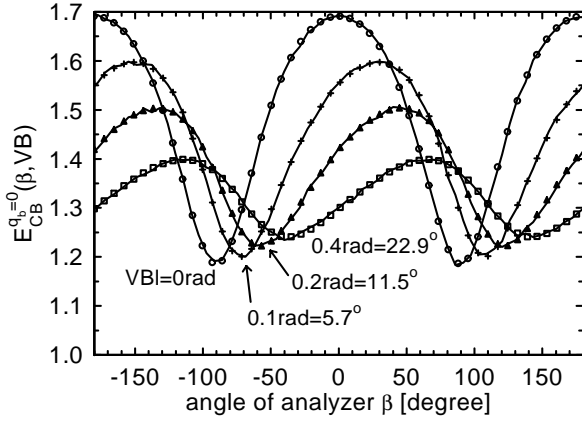
Fig. 7. Rayleigh scattering, linear polarization, $\mathbf{B} \parallel \mathbf{k}_{\mathrm{in}}$, $\ell_a = 100\ell^\star$. Solid lines: Monte-Carlo simulation of E_{CB} for different values of FR in the exact backscattering direction while the analyzer is twisted by an angle β. Dots: fits according to equation (31). The fit parameters $\frac{I_{\mathrm{ms}}}{I_{\mathrm{ms+ss}}} \overline{\mathcal{C}}$, $\xi_{1,2}$, β'_{ms} and $\beta'_{\mathrm{ms+ss}}$ are magnetic field dependent.

between these two points can be treated in the diffusion limit. With these assumptions one obtains for the angle between polarizer and analyzer for which the CB cone is maximal: $\beta'_{\mathrm{ms}} = \arctan(2VB\ell_\beta)$ with $\ell_\beta = \ell^\star_{\mathrm{FR}}$. For small values of $VB\ell_\beta$, the linear approximation of $\beta'_{VB\to 0}$ is equal to $2VB\ell_\beta$, independent of the exact distribution of the starting and end points (*i.e.* independent of approximation (ii)), only the average value is important. The polarization of the incoherent multiple scattered intensity has its maximum at the same angle β'_{ms}. However, this is not the case for the single scattered intensity where beginning and end points are the same lying at an average depth of ℓ inside the sample. For the single scattering intensity one finds $\beta'_{\mathrm{ss}} = \frac{1}{2}\arctan(2VB\ell)$. Moreover, its polarization is smeared out (*i.e.* $I^\pm_{\mathrm{ss}}$ is no longer zero) due to the fluctuations of the position of the first scattering events; with increasing FR one finds that the difference between its maximum and minimum value decreases as $I^{ss}_{VB=0}/\sqrt{1+(2VB\ell)^2}$. Figure 7 shows a simulation of E^{xx}_{CB} where the analyzer was twisted by an angle β *versus* the polarizer. Without FR, the CB enhancement in the exact backscattering direction as a function of β is given by [27]:

$$E^{q_{\mathrm{b}}=0}_{\mathrm{CB}}(\beta) = 1 + \frac{I^{xx}_{\mathrm{ms}}\mathcal{C}^{xx}\cos^2\beta + I^{xy}_{\mathrm{ms}}\mathcal{C}^{xy}\sin^2\beta}{I^{xx}_{\mathrm{ms+ss}}\cos^2\beta + I^{xy}_{\mathrm{ms+ss}}\sin^2\beta}. \quad (30)$$

Without FR, $\mathcal{C}^{xx}$ is equal to 1 and I^{xy}_{ss} is zero. With FR, the expressions $\mathcal{C}^{xx}$, I^{xx}_{ms}, I^{xx}_{ss} etc. become magnetic field dependent and the multiple scattered parts are shifted by an angle $\beta \to \beta - \beta'_{\mathrm{ms}}$ whereas I^{xx}_{ss} and I^{xy}_{ss} are shifted by β'_{ss}. The simulated curves in Figure 7 were fitted to the equivalent expression (now, the VB dependence is included):

$$E^{q_{\mathrm{b}}=0}_{\mathrm{CB}}(VB,\beta) = 1 + \frac{I_{\mathrm{ms}}}{I_{\mathrm{ms+ss}}}\overline{\mathcal{C}}\frac{1 + \xi_1\cos[2(\beta - \beta'_{\mathrm{ms}})]}{1 + \xi_2\cos[2(\beta - \beta'_{\mathrm{ms+ss}})]}. \quad (31)$$
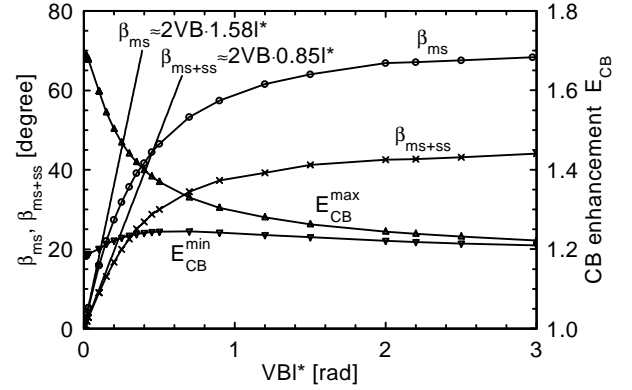
Fig. 8. Evaluation of Figure 7. Maximum and minimum values of E_{CB} as a function of FR as well as the according phases (*i.e.* rotations) of the multiple scattered and single plus multiple scattered intensities. The functions $\beta'[VB\ell^\star]_{\mathrm{ms}}$ and $\beta'[VB\ell^\star]_{\mathrm{ms+ss}}$ are characteristic for a sample, *i.e.* type of scatterers, index of refraction etc. and depend on the propagation of light in a surface layer of thickness $\approx \ell^\star$. $E^{\mathrm{min}}_{\mathrm{CB}}$ increases for smaller values of VB due to the fluctuations of the starting and end points of the light paths in the sample.

The parameters $\xi_{1,2}$ and $\beta'_{\mathrm{ms+ss}}$ depend on the corresponding parameters of equation (30). In the simulations, as expected, the maximum is shifted by an angle to the order of $2VB\ell^\star$ with increasing FR. Moreover, according to equations (30, 31), it can be observed that these curves are not just cosines and even become asymmetric with FR due to the fact that $\beta'_{\mathrm{ms+ss}}$ is smaller than β'_{ms}. Quantitatively (see Fig. 8), we find values for ℓ_β of $0.79\ell^\star_{\mathrm{FR}}$ for the multiple scattered and $0.43\ell^\star_{\mathrm{FR}}$ for the single plus multiple scattered part. These quantitative differences may be explained by the simplifications (i)-(iii) further above. In fact, it is for example not true that the distribution of the starting and end points is exponential: the incoming light is convoluted with the probability for single scattering which does not contribute to CB and the outgoing light is convoluted with the intensity distribution close to the surface. In order to illustrate this effect, we incorporated the refractive index n of the sample into our simulations. Due to the internal reflections, the amount of single scattering decreases and the light intensity near the surface increases. For a sample with $n = 1.6$ we found the values $\ell^{\mathrm{ms}}_\beta = 0.675\ell^\star_{\mathrm{FR}}$ and $\ell^{\mathrm{ms+ss}}_\beta = 0.435\ell^\star_{\mathrm{FR}}$. For Rayleigh-Gans-Debye scattering we again found different values of ℓ_β.

We insisted quite strenuously on this case because it is possible this way to study the influence of the surface on the scattering experimentally. Theoretically at least, this problem is in no way trivial.

3.2 Rayleigh-Gans-Debye scattering

In the case of circular polarization and magnetic field parallel to the incident light (no figure), the result is quite similar to the result for Rayleigh scattering. However, CB is only destroyed to some extent. In fact, the larger the ratio of $\ell^\star/\ell$ the smaller is the influence of FR on CB.
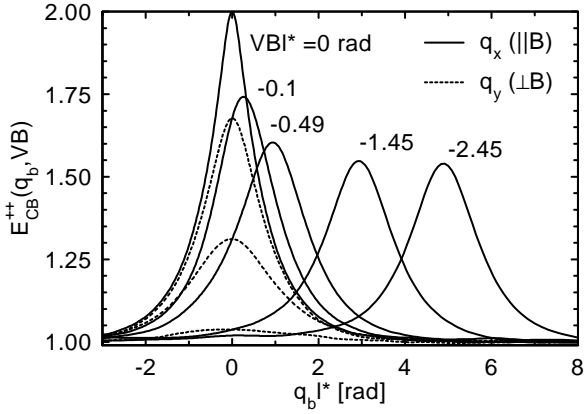
Fig. 9. Monte-Carlo simulation of E_{CB} as a function of $q_b\ell^\star$ for Rayleigh-Gans-Debye scattering, size parameter $ka = 3$, i.e. $\ell^\star/\ell = 4.9$, circular polarization, $\mathbf{B} \perp \mathbf{k}_{in}$ and $\ell_a = 100\ell^\star$. The cone is destroyed only to some extent and shifted by an angle $2V\mathbf{B}\ell^\star$ in direction of the magnetic field (solid lines).

This same result has already been encountered by Martinez & Maynard. Figure 9 shows the result for E_{CB}^{++} with the magnetic field perpendicular to the incident light. Here, the maximum is shifted in direction of the magnetic field by the angle $2VB\ell^\star$. This is due to the fact that with Rayleigh-Gans-Debye scattering the circular depolarization is rather minor, i.e. $\ell_{p,c}$ is much longer than $\ell^\star$ (see Fig. 3). For the part of the light that is not depolarized, the phase shift α_{FR} is $V\mathbf{B} \cdot \mathbf{r}'$, where $\mathbf{r}'$ is the distance between beginning and end points of the light paths. Therefore, in equation (16), $\mathbf{q}_b$ can be replaced by $\mathbf{q}_b + 2\sigma V\mathbf{B}$, which corresponds to a shift of the cone[1].

Figure 10 shows the result for E_{CB}^{xx} in the same geometry. This time, two maxima appear with increasing FR at $\mathbf{q}_b = \pm 2V\mathbf{B}$. This can be explained by decomposing the linear polarization into the two circular polarized states, which experience a phase shift according to the case '++', but of opposite sign. The height of these maxima corresponds, as expected, to roughly half of the height of the maximum in the case '++', which is also about the height of the persisting cone, in the case where the field is parallel to the incident light.

The appearance of secondary maxima and the asymmetry of the cone in the case of Rayleigh scattering can be explained, to some extent, similarly to the case of Rayleigh-Gans-Debye scattering. However, especially in

---

[1] There is another (relativistic) phenomenon analogous with the experiment of Fizeau [28], which introduces a different phase shift ϕ between the direct and reversed paths: if the bulk material is moving with the velocity $\mathbf{v}$, both paths differ by the phase $\Delta\phi \simeq 2k_o\mathbf{v}/c_o \cdot \mathbf{r}' (n^2 - 1)$, where k_o is the wave vector in air, c_o the velocity of light in air, n is the refractive index of the sample and $\mathbf{r}'$ is the distance between beginning and end point of the random walk. However, this phase shift is correlated with $\mathbf{q}_b \cdot \mathbf{r}'$ and will only change the direction of the maximum by a scattering vector $\mathbf{q}_v = 2k_o(\mathbf{v}/c_o)(1 - n^2)$, i.e. the maximum is no longer in the exact backscattering direction.
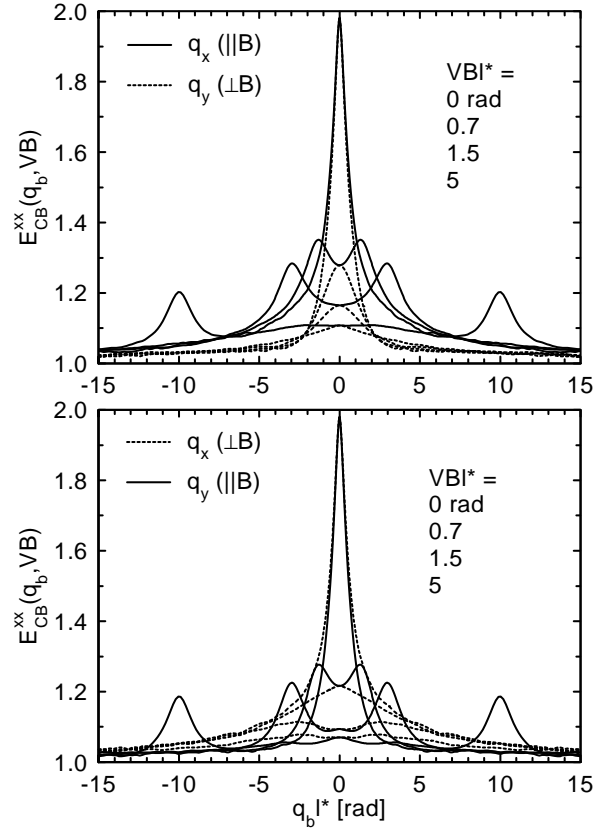
Fig. 10. Same situation as in Figure 9 but for the case 'xx'. The remaining cone is shifted in the directions $\pm 2V\mathbf{B}\ell^\star$. Note that in the lower graph, essentially for $VB\ell^\star = 1.5$, there are also two maxima in the directions $q_b \perp B$.

the case '++' and $\mathbf{k}_{in} \perp \mathbf{B}$, an additional effect appears which can be better understood by using the random helicity flip model where the 'scatterers' only flip the polarization between the two circular eigen-states, randomly: after the first scattering event, the light is in one of the two circular polarization states with the same probability. After the first scattering event there is a certain probability that there will be no further helicity flips on the rest of the light path with exception of the last scattering event. Consequently the light experiences a phase shift $\alpha_{FR} = \pm V\mathbf{B} \cdot \mathbf{r}$ which corresponds to a shift of the cone in the direction of $\mp\mathbf{B}$. The height of these two maxima corresponds to the probability of those light paths. This is the explanation for the secondary maxima in Figure 5. They are smaller than in the case of the helicity flip model because of depolarization and correlations of the circular polarized states.

3.3 Summary

The results we obtained in our simulations correspond quite well, qualitatively, to the results and predictions we have made in the theoretical section. It is evident that there is no quantitative coincidence as the backscattering geometry (half infinite space) implies a strong

Table 1. Simulated values of E_{CB} in the exact backscattering direction at zero magnetic field and for $VB\ell^\star \to \infty$. If $I_{ss} \neq 0$ the values of $\mathcal{C}$ are given in brackets; $\mathbf{k}_{\text{in}} \parallel \mathbf{B}$, $\ell_a = 100\ell^\star$, error 5%. In the case of linear polarization, the simulations are evaluated as described in Figures 7 and 8. For Rayleigh scattering, E_{CB}^{xy} passes through a maximum.

		circular		linear	
	++	±		max	min
R a y l e i g h	2	1.309 (0.463)		1.692	1.185
	↓	$VB\ell^\star$ ↓ ↓ ∞		↓	1.246 (0.326)
	1.068	1.224 (0.343)		1.17 (0.221)	
R G D $ka = 3$	2	1.156 (0.159)		1.981	1.18
	↓	↓		↓	
	1.52	1.114 (0.117)		1.335 (0.339)	

restriction on the light paths. Apart from the comparisons between simulations and theory we have made, we also intend to give a short discussion of the results that we were not able to display here explicitly (see also Tab. 1).

As already mentioned above, in the case of Rayleigh-Gans-Debye scattering, CB is destroyed to only some extent. Also with Rayleigh scattering, the cone is never completely destroyed. In the case $\mathbf{B} \perp \mathbf{k}_{\text{in}}$, for example, the coherent part of double scattering is not destroyed by FR because the scattering matrices of the direct and the reversed paths, FR included, are the same.

In the cases 'xx' and 'xy', in the limit of $VB\ell^\star \to \infty$, the CB enhancements decrease to the same value (see Tab. 1) what was predicted by equations (26, 27). For circular polarization, different values for '++' and '±' are expected. We found values of 1.22 and 1.07, respectively, in the case of Rayleigh scattering. For Rayleigh-Gans-Debye scattering ($ka = 3$), $\mathcal{C}^+$ is only destroyed to 50% due to the relatively weak circular depolarization. $\mathcal{C}^\pm$ was predicted to be unchanged by FR what is more or less fulfilled in case of Rayleigh-Gans-Deby scattering.

It is also interesting to note that for Rayleigh-Gans-Debye scattering, in the case 'xy', $\mathbf{B} \perp \mathbf{k}_{\text{in}}$, relatively large secondary maxima appear. For the sample of Figure 9 one finds at zero field, in the exact backscattering direction, $E_{\text{CB}}^{xy} = 1.178$ and at $VB\ell^\star \gtrsim 2$, $E_{\text{CB}}^{xy}(\mathbf{q}_\text{b} = \pm 2V\mathbf{B}) = 1.135$, i.e. the sum of the coherent part of the side maxima is larger than the cone at zero field.

Moreover, the simulations confirmed, e.g. for small values of $VB\ell^\star$, that the influence of FR on CB is greater for Rayleigh than for Rayleigh-Gans-Debye scattering, according to the different values of $\ell_{\text{FR}}^\star$.

4 Experiments

Faraday rotation is present in any material, but in most cases it is very small. To study the influence of FR on CB and in order to considerably influence CB, the product of the three parameters $2VB\ell^\star$ must be on order unity.
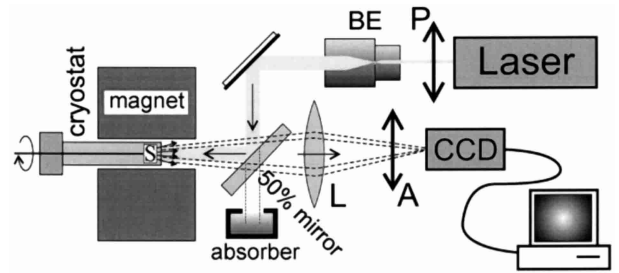
Fig. 11. Experimental setup to measure the CB cone at high magnetic fields. The sample (S) (diameter ≈ 13 mm, thickness ≈ 5 mm) was placed in an optical cryostat at temperatures down to 30 K. It was rotated to average over many speckle patterns. The cryostat window of the sample chamber was mounted on a very thin steel tube in order to reduce birefringence. The cryostat was inserted into the magnet hole which had a diameter of 50 mm (magnetic field parallel to the hole). Laser: linear polarized Ar^+-Laser at 457.9 nm. A beam expander (BE) is used to enlarge the laser beam to about 1 cm and to minimize the divergence of the beam. The semi-transparent mirror is wedge-shaped (diameter = 50 mm). The lens (L) had focal lengths between 250 mm and 500 mm. The analyzer (A) was composed of a $\lambda/4$-plate and a linear polarizer (Polaroid foil) and the polarizer (P) included a Babinet-Soleil compensator such that any incident and detected polarization state could be chosen. In particular we could compensate for the depolarization by mirrors, windows etc. The CCD camera had a resolution of 512×512 pixel of 1 byte. With the PC we averaged over 255 angle resolving pictures. The distance between sample and mirror measured about 0.5 m.

The experiments were carried out at the High Magnetic Field Laboratory, Grenoble, in a resistive magnet with a magnetic field $\mathbf{B}$ up to 23 teslas. The samples which were used, were essentially fabricated of a Faraday rotating glass powder with a Verdet constant V of about $90°$/mm/tesla at 30 K. To produce a significant effect under these conditions the third parameter $\ell^\star$ must be approx. 50 μm or, in other words, the width of the cone must be in the order of $2VB\lambda/2\pi \approx 0.1°$. In our case, depending on the sample, the transport mean free path $\ell^\star$ varied from about 10 μm to 300 μm.

4.1 Experimental setup

Figure 11 shows our experimental setup to measure the CB cone in the presence of a high magnetic field. The measured values of the CB enhancement were always below 1.8 which can be explained by the extreme experimental conditions, e.g. an optical cryostat was necessary in order to perform the measurements at low temperatures. This way we achieved a resolution of about 5×10^{-5} radian which was not quite sufficient to resolve the very peak of the cone. We tested the stability of the cone against experimental artifacts with samples such as Teflon, which have a very low FR. For circular polarization the fluctuations of the CB enhancement were less than 3%. In the case of linear polarization we had to compensate for the FR in the windows of the cryostat but the error was still less than 5%. Unfortunately, with this experimental setup,
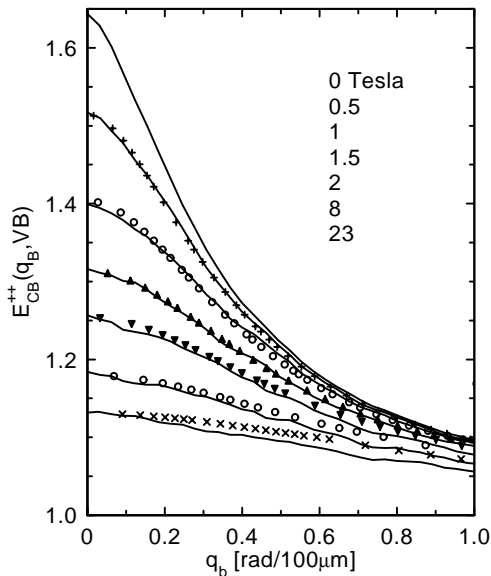
Fig. 12. Solid lines: CB cone '++' for different magnetic field values. Same sample as in Figure 1; temperature 30 K. The curves were obtained by averaging the pictures from the CCD camera in the azimuthal angle of $\mathbf{q_b}$ around the maximum of the cone. Dots: curves which were obtained after rescaling the curve at 0 tesla by $q_b^2 \rightarrow q_b^2 + q_{FR}^2$, where q_{FR} is given by the value at $q_b = 0$.

it was not possible to measure the case where the magnetic field is perpendicular to the incident light.

4.2 Samples

We used a paramagnetic glass as a basic material [29], containing about thirty weight per cent of Tb^{3+}-ions. It has a paramagnetic FR of $-9.25°/mm/tesla$ at room temperature and $-81°/mm/tesla$ at 30 K using a wavelength of $\lambda = 457.9$ nm. Its Verdet constant is magnetic field dependent and tends to a saturation rotation of about $-820°/mm$. The index of refraction is $n = 1.7$. We ground this glass and obtained a white powder of particles with very irregular shapes and sizes between 1 μm and 50 μm. The powder alone has a volume fraction of about 64% of FR material and a transport mean free path $\ell^\star$ of about 40 μm. In order to increase $\ell^\star$ and/or to obtain solid samples we mixed this powder with paraffin, or melted (sintered) the glass powder. The molten samples consisted of about 90% FR material and 10% air cavities in between, and were quite transparent. Therefore, we added one to five volume per cent of non-melting colloidal particles of SiO_2 or TiO_2. Finally, we obtained white samples with values of $\ell^\star$ between 20 and 100 μm. These values were obtained by comparison with Monte Carlo simulations of the cone. For all samples the CB cones in the opposite polarization channels were very small, *i.e.* in the order of 1% and there was no significant difference between E_{CB}^{++} and E_{CB}^{xx}. This means that the depolarization lengths are relatively small, which is not astonishing, as the samples mainly consisted of (sintered) glass particles.
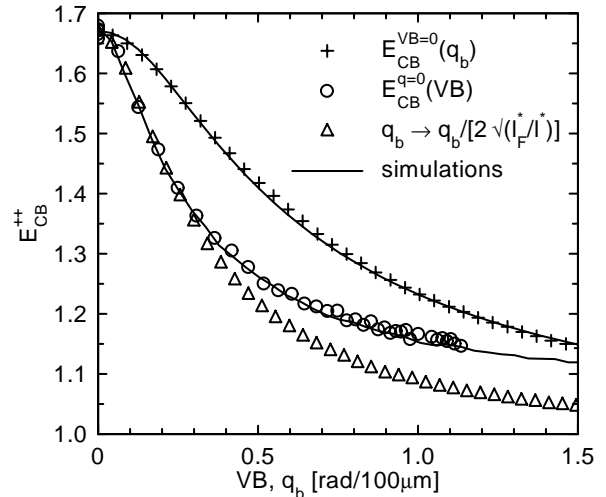
Fig. 13. Marks $(+, \bigcirc, \triangle)$: experimental curves of E_{CB} as a function of q_b at zero field and as a function of VB in the exact backscattering direction. Lines: simulated curves for $\ell^\star = 48$ μm and a size parameter $ka = 1.8$, *i.e.* $\ell^\star/\ell = 2.1$ and $\ell_{FR}^\star/\ell^\star = 1.145$. Sample: molten glass powder mixed with 2% SiO_2 ($a = 127$ nm); temperature 30 K, circular polarized light. The rescaled curve '$\triangle$' (with respect to '+') demonstrates the equivalence of q_b and q_{FR} in equation (13) for small arguments. Due to the limited angular resolution of our experimental setup, the peak of the cone is rounded off. Compared to this, the rounding off by absorption is negligible. In our simulations we took into account this effect, as well as the influence of the internal reflections ($\overline{n} = 1.6$) at the surface of the sample.

4.3 Experimental results

Figure 12 shows an example of how FR decreases CB. For small values of $VB\ell^\star$ the shape of the cone can be described by the substitution $q_b^2 \rightarrow q_b^2 + q_{FR}^2$ with $q_{FR}^2 = \ell^\star/\ell_{FR}^\star (2VB\ell_{FR}^\star)^2$. For larger arguments of q_b and $VB\ell^\star$, the measured curves decrease a little quicker than expected by this substitution. This behavior was also found in the simulations (see Fig. 4). The value $\ell_{FR}^\star/\ell^\star$ can be estimated by comparing the decays of $\mathcal{C}(q_b)_{VB=0}$ and $\mathcal{C}(VB)_{q_b=0}$ for minor arguments (see Fig. 13). For the ten different samples we have studied we find values between 0.6 and 1.6. The lowest value of 0.6 was found in a sample where the glass powder was mixed with paraffin. This sample must depolarize the light very quickly so that $\ell_{p,c}$ is smaller than $\ell^\star$. The greatest value was found in a sintered sample which contained 0.1% of scatterers of TiO_2 (radius 130 nm).

We also compared the experimental data with simulations. Of course, the scattering in our samples does not correspond to pure Mie or Rayleigh-Gans-Debye scattering. However, the shape of the cone is mainly determined by the ratio $\ell^\star/\ell$ which can be the same for different kinds of scatterers. Figure 13 shows a comparison between experiment and simulation for a sample of molten glass powder, containing colloidal particles of SiO_2. The curvatures of the simulated curve $E_{CB}^{VB=0}(q_b)$ and essentially of the curve $E_{CB}^{q_b=0}(VB)$ give the size parameter ka. Finally, both curves were rescaled in q_b and VB by the same factor,
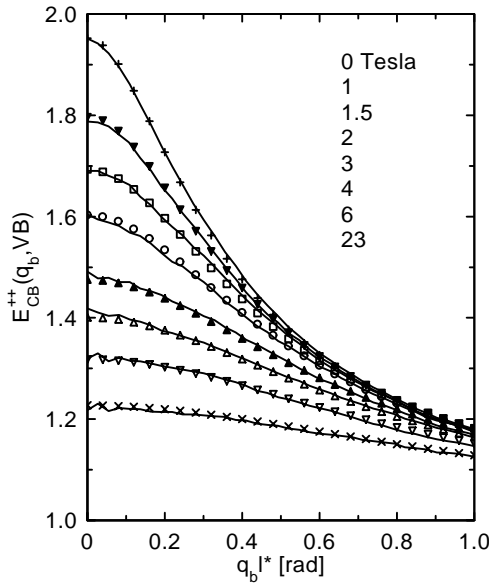
Fig. 14. Solid lines: CB cone for different magnetic field values. Same sample as in Figure 13. Dots: simulated curves using the fit parameters of Figure 13. The experimental curves were rescaled by a factor (same factor for all curves), in such a manner that the peak of the cone at zero field goes up to the theoretical value. This value is slightly less than two, due to the convolution of the simulated curves with the resolution of the experimental setup.

which gives $\ell^\star$. After adjusting these two fit parameters, the coincidence between experiment and simulation is very good. Finally, we simulated with the obtained parameters the whole shape of the cone in presence of FR (see Fig. 14). Again, the agreement is very good.

We also measured the rotation of the linear polarization of the cone in the case 'xx'. In our experiments we could not detect a different rotation of the polarization for the multiple scattered and single plus multiple scattered part of the light, rather only one common shift. For all ten samples the rotation corresponded to a ballistic penetration length of the order of $\ell^\star_{\mathrm{FR}}$, *e.g.* in the case of Figure 13 we find a ballistic length of 45 μm, which is equal to $0.94\ell^\star$ or $0.82\ell^\star_{\mathrm{FR}}$. The simulations for those parameters give a ballistic length of $1.02\ell^\star$.

Apart from this rotation of the polarization we could not find any significant difference between linear and circular polarization in our experiments. In the opposite channels '$\pm$' and 'xy', the cones were very small and, if existent at all, unchanged by FR.

5 Conclusion

We have developed a path model of light which well explains the influence of FR on CB. CB is the direct consequence of the theorem of reciprocity and FR is the only effect (for elastic scattering) which is able to violate reciprocity. However, FR does not necessarily destroy CB. The light needs also to be depolarized. This correlation between CB, FR and the depolarization of light is well

displayed in our model. It turns out that a new characteristic correlation length $\ell^\star_{\mathrm{FR}}$ appears which, for example in the case of Rayleigh scattering, is twice the length of $\ell^\star$. Experimentally, an increased FR effect was also found in speckle correlation measurements including FR [12,30], where it was explained by internal reflections inside the scatterers or by resonant scattering. However, this explanation cannot hold for our kind of samples, where FR is in the bulk material which has a volume fraction of $\approx 90\%$.

Due to the boundary conditions in backscattering geometry, quantitative predictions are very difficult and no longer possible with our model. Therefore, and in order to verify the (qualitative) predictions of our model, we made computer simulations of Monte-Carlo type. These simulations make visible the predicted effects such as the fact that in samples where the circular depolarization is relatively small, CB is not completely destroyed, but the shape of the cone may be changed. Besides, we studied the rotation of the linear polarization of the cone, due to the first and last 'ballistic' step of the light in the sample. This effect can be interesting to study the influence of a boundary on multiple scattering.

We succeeded, in our experiments, in fabricating samples were FR decreases CB considerably. In order to compare the measurements with the simulations, experimental parameters and artifacts such as a limited resolution or internal reflections at the sample surface need to be taken into consideration. In fact, in our case, internal reflections decrease the cone width by about a factor of two. Finally, via these simulations, which matched well with our experiments, we could also verify our model experimentally, at least in the case where the magnetic field is parallel to the incident light.

We hope we succeeded in showing that the study of the influence of FR on CB is an interesting, useful and powerful tool for the characterization, as well as the understanding of the propagation of light in multiple scattering samples.

Appendix: Influence of FR on the scattering

In this work we only considered the influence of FR on the coherent part of the waves, *i.e.* the light which is propagating between two scattering events. Of course, according to the change of the index of refraction by FR, the scattering itself is also influenced: the differential cross section $d\sigma/d\Omega$ changes and becomes asymmetric [31]; even an optical analogue to the Hall effect was reported [32,33]. However, as the change of the index of refraction is very small ($\Delta n = VB\lambda/2\pi \lesssim 10^{-3}$), these effects are negligible in our experiments. In a simple estimation, *i.e.* by calculating the total cross section $\sigma_\pm$ for circular right and left

polarized light respectively, in a sample with the refractive indexes $n_{\pm} = n \pm \Delta n$, we find that the relative change of the scattering mean free path ℓ is about 10^{-5}.

There are two other magneto-optical effects. One is magnetic dichroism which decreases CB as it absorbs circular polarized waves differently, depending on whether they are propagating parallel or antiparallel to a magnetic field. Magnetic dichroism can be described like a FR with a complex angle $\frac{\mathrm{i}\delta a}{2}(\mathbf{B} \cdot \mathbf{r})$ times an attenuation factor $\exp(-ar/2)$, corresponding to the absorption coefficient for the circular right and left polarized intensity given by $a \pm \delta a(\mathbf{B} \cdot \mathbf{r})$. This results in essentially the same equations (25–28), but with another $\mathcal{C}^{+} = (x/\mathrm{arctanh}[x])^{n}$, where $x = B\ell_{\mathrm{FR}}^{\star}\delta a/(1 + a\ell_{\mathrm{FR}}^{\star})$. However, in our samples, absorption and magnetic dichroism are negligible.

The other magneto-optical effect is the Voigt effect which is the analogue to the Cotton-Mouton effect in liquids. Due to the magnetic field the material becomes birefringent. For our bulk material we measured a phase shift of $-0.038°/\mathrm{mm/tesla}^{2}$ at room temperature and $\lambda = 457.9$ nm, $i.e.$ at low magnetic fields the Voigt effect is two orders of magnitude smaller than FR. For higher magnetic fields the Voigt effect becomes more important because of its B^{2} dependence. But the Voigt effect also saturates in paramagnetic materials. In a classical spin model we estimated the saturation phase shift to $-515°/\mathrm{mm}$. Quite apart from that, the Voigt effect does not influence the enhancement factor of CB (it may only effect the shape of the cone) as birefringence does not violate the theorem of reciprocity.

Finally, we have also studied whether the scattering changes the FR of the bulk material. For that, we have measured the FR of the coherent, $i.e.$ non-scattered wave in transmission through thin slights of our samples. As expected, we found that the FR just corresponded to the volume fraction of the FR material in the samples.

References

1. G. Bergmann, Phys. Rep. **107**, 1 (1984).
2. M.P. van Albada, A. Lagendijk, Phys. Rev. Lett. **55**, 2692 (1985).
3. P.-E. Wolf, G. Maret, Phys. Rev. Lett. **55**, 2696 (1985).
4. D.S. Saxon, Phys. Rev. **100**, 1771 (1955).
5. D.S. Wiersma, M.P. van Albada, A. Lagendijk, Rev. Sci. Instrum. **66**, 5473 (1995).
6. R. Lenke, G. Maret, *Multiple Scattering of Light: Coherent Backscattering and Transmission* in *Scattering in Polymeric and Colloidal Systems*, edited by Wyn Brown, Kell Mortensen (Gordon and Breach, Reading U.K., 2000), pp. 1-72.
7. R. Lenke, G. Maret, Progr. Colloid Polym. Sci. **104**, 126 (1997).
8. P.W. Anderson, Philos. Mag. B **52**, 505 (1985).
9. A.A Golubentsev, Sov. Phys. JETP **59**, 26 (1984).
10. F.C. MacKintosh, S. John, Phys. Rev. B **37**, 1884 (1988).
11. R. Lenke, thesis, University of Joseph Fourier-Grenoble I, France, 1994.
12. F.A. Erbacher, R. Lenke, G. Maret, Europhys. Lett. **21**, 551 (1993).
13. R. Lenke, G. Maret, Phys. Scr. **T49B**, 605 (1993).
14. R. Lenke, G. Maret, *OSA Proceedings on Advances in Optical Imaging and Photon Migration* **21**, edited by R.R. Alfano, (Optical Society of America, 1994), pp. 16-19.
15. A.S. Martinez, thesis, University of Joseph Fourier-Grenoble I, France (1993); and private communications.
16. A.S. Martinez, R. Maynard, Phys. Rev. B **50**, 3714 (1994).
17. J.C. Dainty, *Laser Speckle and Related Phenomena*, Topics in Applied Physics **9** (Springer-Verlag, Heidelberg, 1984).
18. More precisely, the vector $\mathbf{r}'$ lies in a surface layer of thickness $\approx \ell$ (scattering mean free path). As the CB cone is very narrow, normally, and due to symmetry reasons, $\mathbf{q}_{\mathrm{b}}$ is well approximated by its part perpendicular to $\mathbf{k}_{\mathrm{in}}$ and $\mathbf{r}'$ by its part parallel to the surface.
19. P.E. Wolf, G. Maret, E. Akkermans, R. Maynard, J. Phys. France **49**, 63 (1988).
20. E. Akkermans, P.E. Wolf, R. Maynard, G. Maret, J. Phys. France **49**, 77 (1988).
21. With the exception of point like scatterers and scattering mean free paths $\ell \gg \lambda$, the differentiation between single and multiple scattering is not trivial. For larger scatterers ($\gg \lambda$), CB happens already inside one single scatterer, $i.e.$ participates to the form factor [22]. In many materials like polymers, for example, where the scattering is caused by fluctuations of the index of refraction, distinct scatterers cannot even be defined. Appart from single scattering, also loops of light paths starting and ending at the 'same scatterer' do not contribute to CB [23]. The weight of these light paths, however, becomes only relevant for very strongly scattering media ($\ell^{\star}$ of the order of the wavelength λ). Again, like in the case of single scattering, the question arises about the size of the 'same scatterer'. The relevant distance should be of order λ because this is the distance beyond which two point like scatterers can be regarded as independent when illuminated by a plane wave and because λ is the extension of one mode (which is the coherence area of the light) inside a multiple scattering media.
22. R. Lenke, U. Mack, G. Maret, *Comparison between 'The Glory' and Coherent Backscattering of Light in turbid media*, submitted to J. Opt. A: Pure Appl. Opt.
23. D.S. Wiersma, M.P. van Albada, B.A. van Tiggelen, A. Lagendijk, Phys. Rev. Lett. **74**, 4193 (1995).
24. Note that $e_{\otimes} = |e_{\otimes}| \exp[\mathrm{i}(\varphi + \alpha_{\mathrm{FR}})]$, $e_{\odot} = |e_{\odot}| \exp[\mathrm{i}(\varphi - \alpha_{\mathrm{FR}})]$ where φ is a phase of no importance.
25. H.C. van de Hulst, *Light Scattering by Small Particles* (Dover Publications, New York, 1957).
26. A. Heiderich, thesis, University of Joseph Fourier-Grenoble I, France, 1995.
27. Strictly speaking, this linear superposition of $\mathcal{C}^{xx}$ and $\mathcal{C}^{xy}$ is only correct for a rotational invariant sample, with respect to $\mathcal{P}_{\mathrm{l}}$.
28. J.D. Jackson, *Classical Electrodynamics* (John Wiley & Sons, New York, 1962).
29. Terbium Borosilicate Glass *FR-5*, manufacturer *Hoya*.
30. F.A. Erbacher, thesis, University of Konstanz, Germany, 1992.
31. B.A. van Tiggelen, R. Maynard, T.M. Nieuwenhuizen, Phys. Rev. E **53**, 2881 (1996).
32. G.L.J.A. Rikken, B.A. van Tiggelen, Nature **381**, 54 (1996).
33. A. Sparenberg, G.L.J.A. Rikken, B.A. van Tiggelen, Phys. Rev. Lett. **79**, 757 (1997).